Nuclear Instruments and Methods in Physics Research A 618 (2010) 131–138

Contents lists available at ScienceDirect

Nuclear Instruments and Methods in Physics Research A

journal homepage: www.elsevier.com/locate/nima

Analytic model of thermal runaway in silicon detectors

Graham Beck [a], Georg Viehhauser [b,*]

[a] Department of Physics, Queen Mary University of London, Mile End Road, London E1 4NS, UK
[b] Particle and Nuclear Physics, Oxford University, Keble Road, Oxford OX1 3RH, UK

ARTICLE INFO

Article history:
Received 26 January 2010
Received in revised form
24 February 2010
Accepted 25 February 2010
Available online 4 March 2010

Keywords:
Silicon detector
Thermal runaway
Thermal management
Cooling

ABSTRACT

Usually the thermal behavior of silicon detectors is predicted from numerical methods (FEA or finite difference methods). However, these results are specific to the modelled structure and the input parameter set. Here we pursue the complementary, analytic, approach which offers some general (if approximate) results that allow relatively simple extrapolation of the performance of a specific detector design.

We present simple network models to calculate analytically the limit of thermal stability in silicon detectors. In particular we use a minimal model, which ignores the thermal resistance within the sensor in comparison with the off-detector resistance. We further discuss an extension of this model to study the effects of a finite sensor thermal resistance.

1. Introduction

One of the consequences of radiation damage in silicon sensors is an increase in leakage current, which depends linearly on the sustained fluence [1]. The resulting heat from the sensor, together with the heat from on-detector electronics, needs to be removed from the low-mass detector structures to avoid thermal damage. Understanding this heat transfer is critical for the detector design as well as for the design of the cooling system, which in typical applications at present and future high-luminosity hadron machines has to provide cooling well below 0 °C.

This understanding is complicated by the strong temperature dependence of the sensor leakage current $I \propto T^2 \exp(-E_g/2kT)$, and hence the leakage power, which in turn affects the temperature according to the thermal resistance of the heat paths. Usually the thermal behavior of the detector is predicted from numerical methods (FEA or finite difference methods) which are able to model the complex structures. However, purely numerical results tend to obscure trends or give little insight into their origins, and the results are specific to the modelled structure and the input parameter set. Here we pursue the complementary, analytic, approach which offers useful insight and some general (if approximate) results that allow relatively simple extrapolation of the performance of a specific detector design.

The thermal behavior of silicon detectors has traditionally been studied for the case of excellent thermal contact to a sink (coolant) along one or two edges. In this case the thermal resistance is defined by the thermal conductivity of the silicon [2,3]. This is the typical situation for detectors at e^+e^- colliders, with extended sensor ladders and the electronics and cooling towards the end. After the issue of thermal runaway was appreciated, in particular for detectors at high-luminosity hadron colliders, detector design strived to reduce sensor thermal resistances making use of progress in material sciences (thermal pyrolitic graphite (TPG), carbon–carbon, high-conductivity ceramics, etc.) [4,5], while reducing the distance over which the heat is conducted on the sensor. At the same time space and material requirements, as well as constraints from the assembly in real detector systems, result in relatively significant resistances from the sensor to the sink. Therefore, in such systems the ratio of internal to external thermal resistance is typically small and the temperature within the sensor tends to be uniform compared to its rise above the coolant temperature. This allows for a simplification of the problem which has been used in Ref. [6] and will also be the starting point for this paper.

The thermal characteristic of a silicon detector system has several implications on its performance. First, the system can become thermally unstable (“thermal runaway”), if the heat generated in the detector exceeds the cooling capacity of the system. Estimates of the headroom (margin of operation) in terms of coolant temperature and radiation induced power are of major concern and in the following we will try to understand how to predict and relate them. A second consideration is the leakage current per detection element (strip or pixel). This will give rise to a shot noise contribution according to [7]

$$ENC_{shot}/[e] \approx \sqrt{12\left[\frac{1}{\mathrm{nA}\cdot\mathrm{ns}}\right] I\tau} \quad (1)$$

where I is the leakage current in the detection element and τ the signal shaping time. The noise contribution from shot noise usually should not exceed the noise from other sources in the

* Corresponding author. Tel.: +44 1865 273410.
E-mail address: g.viehhauser1@physics.ox.ac.uk (G. Viehhauser).

0168-9002/$ - see front matter © 2010 Elsevier B.V. All rights reserved.
doi:10.1016/j.nima.2010.02.264

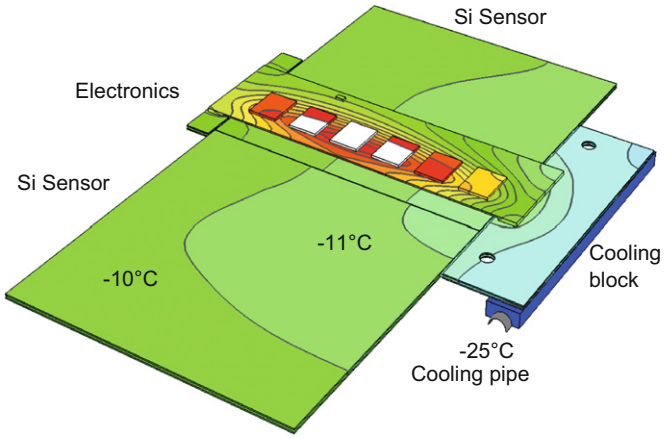

Fig. 1. Thermal FEA of ATLAS barrel SCT Silicon strip module (top plane with two $6\times6\,cm^2$ sensors visible) with a hybrid power of 6 W and a sensor leakage power of $120\,\mu W/mm^2$ at 0 °C. Temperatures range from −25 (coolant) to +6° (electronics maximum). Contours are shown at 1 °C intervals between −20 and +4 °C. Note the small variation of temperature (labelled contours) over the sensor surface.

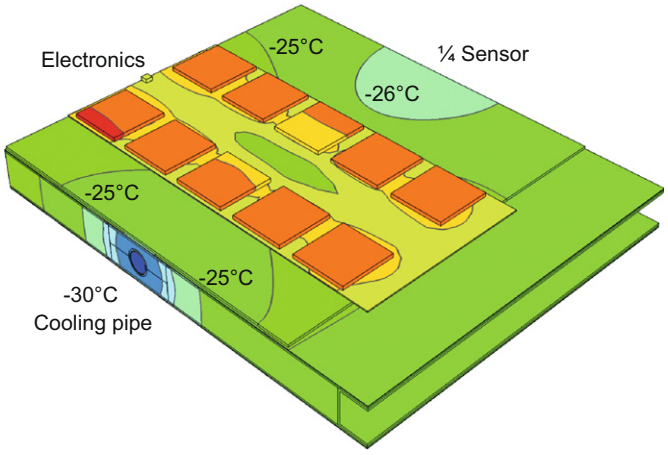

Fig. 2. ATLAS upgrade short strip barrel module: thermal FEA of one quarter of the module area with an assumed hybrid power per sensor of 6 W and sensor leakage power of $1000\,\mu W/mm^2$ at 0 °C. Temperature contours (labelled on the sensor) range from −30 (coolant) to −20 °C (electronics maximum) at 1 °C intervals.

system, thus putting a constraint on the sensor leakage current. Finally, the total leakage power and currents in the detector have implications on the specification of the bias voltage supply system. Ultimately, any failure to address these issues will result in a reduction of the achievable signal-to-noise (S/N) ratio and thus jeopardize the performance of the system.

We will illustrate our model on the ATLAS barrel SCT modules [8], and the stave design envisaged for the sLHC ATLAS strip tracker upgrade [9]. However, our models are generally applicable.

The ATLAS barrel SCT module (Fig. 1) has two planes of silicon sensors, each bridged by an electronics hybrid on a carbon–carbon carrier. The two planes are glued back-to-back onto a TPG baseboard [5], which extends to a cooling block. The cooling block is soldered onto the cooling pipe. The thermal interface between the baseboard and the cooling block is provided by thermal grease.

In the design suggested for the sLHC ATLAS strip tracker upgrade (Fig. 2) the silicon sensors ($10\times10\,cm^2$) are bonded onto a carbon fibre-honeycomb sandwich with two embedded cooling pipes. The cooling pipes are encapsulated by a carbon foam of high thermal conductivity (POCOFoam [10]). The electronics hybrids are glued directly onto the silicon sensor. This design bonds the components (structure, sensor and hybrid) much closer with larger contact areas than in the present ATLAS SCT modules. The cooling pipe is closer to the heat sources, thus reducing the resistance of the thermal path to the sink, and the heat paths for the two sides are separated, in contrast to the ATLAS barrel SCT module.

2. Temperature dependence of sensor power

Throughout this paper we assume uniform radiation damage over the surface of the sensor and fixed bias voltage and depletion depth. We use the conventional approximation for the dependence of leakage current on the (in general position dependent) sensor temperature $T_S^2\exp(-E_g/2kT_S)$ where the quadratic term accounts for thermal velocity and density of states and E_g is an effective energy gap for carrier generation, empirically ~1.2 eV for radiation damaged silicon. For convenience we denote $E_g/2k$ by T_A (*A*ctivation *T*emperature). Then the power Q dissipated in the sensor varies as

$$Q\sim T_S^2 e^{-T_A/T_S} \tag{2}$$

where $T_A\approx7000$ K, which is very much greater than the sensor operating temperature.

It is straightforward to differentiate Eq. (2), giving

$$\frac{\partial Q}{\partial T_S}=\frac{2T_S+T_A}{T_S^2}\times Q. \tag{3}$$

We can write Q in terms of the power Q_{ref} dissipated at a reference temperature T_{ref}

$$Q(T_S)=Q_{ref}\left(\frac{T_S}{T_{ref}}\right)^2\exp\left(T_A\left(\frac{1}{T_{ref}}-\frac{1}{T_S}\right)\right). \tag{4}$$

T_{ref} is often taken as 0 °C and Q_{ref} at that temperature estimated from empirical knowledge of the radiation induced leakage current and operational bias voltage.

3. Minimal model

In order to treat thermal runaway analytically we model the silicon sensor as an ideal source of heat $Q(T_S)$ with zero internal thermal resistance (Fig. 3). It is connected to a heat sink (coolant) at constant temperature T_C by a thermally resistive path, which we take to be independent of temperature and heat flux.[1] We account for the heating effect of the readout electronics by adding a temperature-independent source Q_H which shares a section of the thermal path with a common resistance R_C. The resistance of the thermal path unique to the sensor is denoted by R_s. The total resistance for the sensor heat path is $R_t=R_S+R_C$.

In the absence of leakage current ($Q=0$) the hybrid heat raises the sensor temperature by R_CQ_H. We denote the resultant temperature $T_C+R_CQ_H$ by T_0. We remark that, however complex the circuit external to the sensor, in the absence of temperature dependence it can in general be replaced by an appropriate Thévenin equivalent as in Fig. 3(b).

[1] In reality this assumption might not be strictly correct. Some materials display (small) variations of the thermal conductivity with temperature. Also, if the heat sink is provided by evaporative cooling the heat transfer coefficient between the boiling liquid and the cooling pipe wall does depend on the heat flux and the evaporation temperature.

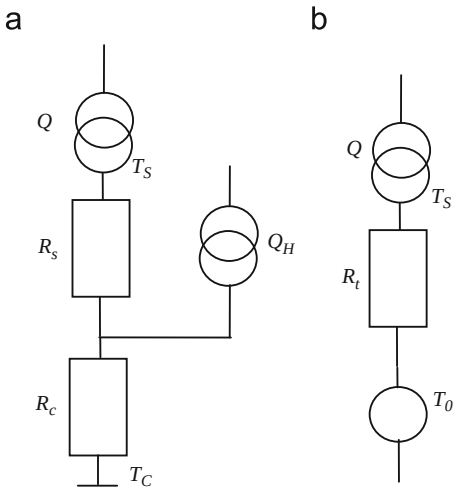

Fig. 3. (a) Minimal model used in this paper and (b) equivalent circuit after introduction of the temperature for zero leakage current T_0.

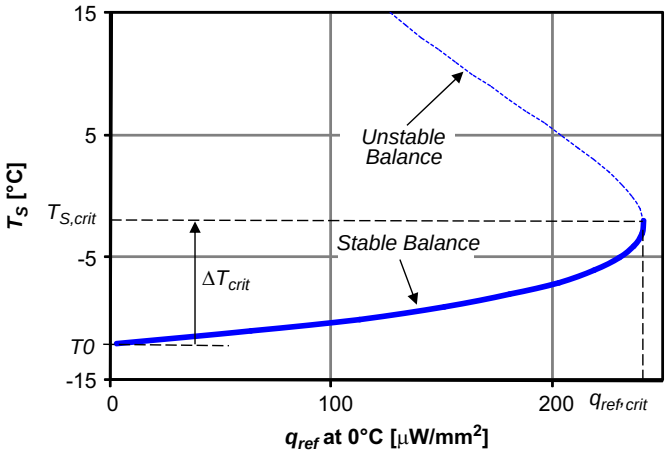

Fig. 5. Sensor temperature versus sensor leakage power for the range of stable operation in the minimal model.

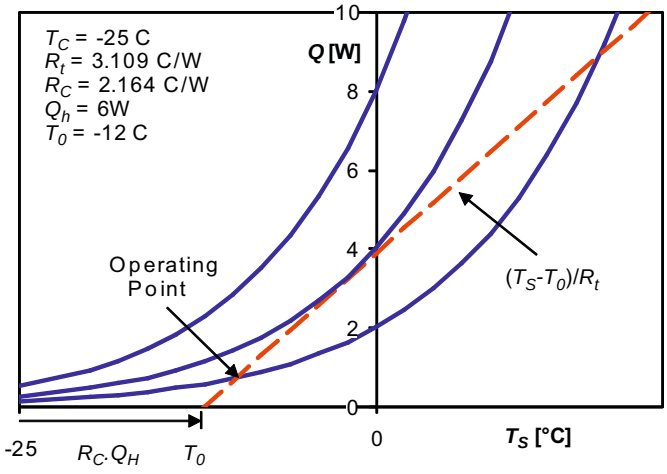

Fig. 4. The balance of dissipated and conducted heat. The curves represent sensor heats of $Q(0\,^{\circ}C)=2$, 4 and 8 W. The dashed line represents conduction by the thermal path. Numerical values are appropriate to the ATLAS SCT barrel module (Fig. 1), with the lowest curve (2 W) corresponding to the maximum expected radiation damage during ATLAS operation.

4. Thermal continuity and runaway

When the sensor is powered its operating temperature T_S satisfies the thermal balance condition

$$Q(T_S) = \frac{T_S - T_0}{R_t}. \tag{5}$$

Fig. 4 illustrates this graphically for different values of Q_{ref}. The thermal balance is given by the intersection of $Q(T_S)$ with the dashed line, which may be termed a load line. The stable operating point for the lowest curve is at the lower temperature intersection (the higher intersection representing an unstable balance). For a higher value of Q_{ref} (about a factor two in this example) the load line is a tangent to the curve, corresponding to the limit of stable operation, which we will denote by $Q_{ref,crit}$. For higher values of Q_{ref} the curve has no intersection with the load line and in this case the system will undergo thermal runaway: the sensor temperature will increase, increasing further the sensor leakage power, and the sensor temperature must run away. It is instructive to consider the effect of changing the coolant temperature or level of electronics heating (which shift the load line along the T axis) and the thermal resistance (which changes its slope).

In order to assess runaway headroom in terms of radiation damage it is usual to plot thermal FEA results for the maximum sensor surface temperature as a function of Q(0C). In the minimal model this curve is obtained from Eqs. (4) and (5) which give the relation

$$Q_{ref} = \frac{(T_S - T_0)}{R_t}\left(\frac{T_{ref}}{T_S}\right)^2 \exp\left(T_A\left(\frac{1}{T_S} - \frac{1}{T_{ref}}\right)\right) \tag{6}$$

We cannot solve[2] this for T_S, but it is straightforward to describe the sensor characteristic by evaluating Eq. (6) over a range of T_S and plotting the results with the axes inverted (Fig. 5). Here we express the power in terms of q, its density per unit area of sensor surface.

The lower (solid) portion of the curve is usually referred to as the "runaway curve", a misleading term since the curve describes the region of *stable* operation. The continuation to the upper (dashed) portion of the curve is of no physical interest but emphasises that the stable region terminates, with infinite slope, at a *finite* temperature, $T_{S,crit}$. We expect that time-independent FEA should yield stable solutions up to a similar, maximum temperature. In order to observe the progress of runaway (beyond that temperature) a time-dependent analysis is required, as shown in Fig. 6. Here the detector is subjected to a sequence of steps in q_{ref}. The temperature stabilises at each step, but after a progressively higher jump, following the behavior of Fig. 5. During the final step (after a total rise of order ten degrees) it runs away.

The response to a perturbation of the power from sensor or electronics is governed by a time constant $\tau = R_t C_p$, with the detector heat capacity C_p. In the minimal model this can be included by adding a capacitor in parallel with the resistive path to the sink. This time constant is typically of the order of a minute for realistic low-mass detector designs. In the stable regime the sensor temperature will adapt on this time scale to a load change, whereas the temperature will run away on this time scale beyond the critical point (Fig. 6).

[2] The lack of a solution to the non-linear, non-homogeneous differential equation describing an extended, resistive sensor was already noted in Ref. [4].

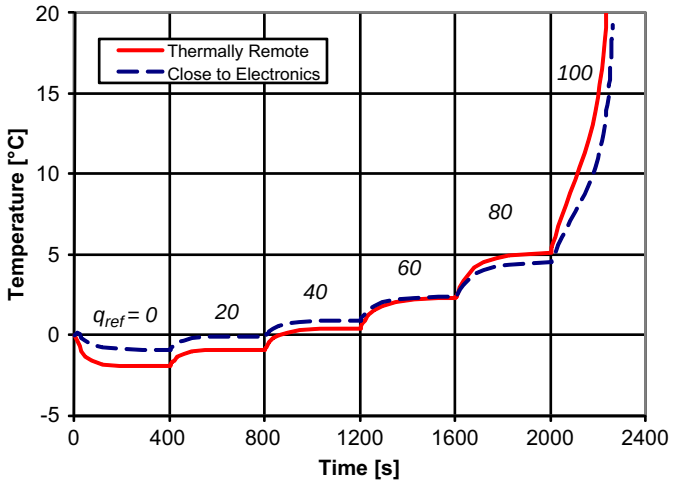

Fig. 6. FEA calculation of the response of the ATLAS SCT barrel module to steps in leakage power of 20 μW/mm^2 (at 0 °C) every 400 s. The dashed curve is for a sensor location close to the electronic hybrid. The solid curve is for the point furthest from the heat sink (coolant at -15 °C).

5. Critical parameters in the minimal model

A perturbation in sensor temperature δT_S changes the heat generated by $(\partial Q/\partial T_S)\delta T_S$ and the heat conducted by $(1/R_t)\delta T_S$. The thermal equilibrium will be stable if $(\partial Q/\partial T_S) < 1/R_t$ and unstable if $\partial Q/\partial T_S > 1/R_t$. The condition of limiting stability, given by setting $\partial Q/\partial T_S$ from Eq. (3) equal to $1/R_t$, results in an equation for the sensor temperature $T_{S,crit}$, above which it is unstable and will run away

$$\frac{2T_{S,crit}+T_A}{T_{S,crit}^2} = \frac{1}{R_t Q} = \frac{1}{(T_{S,crit}-T_0)} \tag{7}$$

so that

$$T_{S,crit}^2 + (T_A - 2T_0)T_{S,crit} - T_A T_0 = 0. \tag{8}$$

The positive $T_{S,crit}$ solution is

$$T_{S,crit} = T_0 + \left(\sqrt{T_A^2 + 4T_0^2} - T_A\right)/2. \tag{9}$$

To first order in $(T_0/T_A)^2$ the maximum temperature rise consistent with stability is hence given by

$$\Delta T_{S,crit} \equiv T_{S,crit} - T_0 \approx T_0^2/T_A. \tag{10}$$

This equation is accurate to better than 0.15% for temperatures below 0 °C.

Over the range of T_0 from −30 to 0 °C, ΔT_{crit} varies from 8.5 to 10.7 °C. In this representation the critical parameters are dependent on the coolant sink temperature, and on the thermal resistance and hybrid heat to the extent that these determine T_0, the temperature of the sensor when there is negligible contribution from leakage current.

From Eq. (10) and the load line relation Eq. (5) the power Q_{crit}, dissipated by the sensor at the limit of stability is given by

$$Q_{crit} = \frac{T_0^2}{R_t T_A}. \tag{11}$$

Hence the corresponding critical leakage power at the reference temperature is given from Eq. (4) by

$$Q_{ref,crit} = \frac{T_A T_{ref}^2}{(T_A+T_0)^2} \exp\left(T_A\left(\frac{1}{T_{S,crit}} - \frac{1}{T_{ref}}\right)\right)/R_t. \tag{12}$$

This equation allows us to estimate, for a given leakage power, the headroom against thermal runaway.

Also, we can find the dependence of the critical leakage power on a change in T_0. To first order in T_0/T_A

$$\frac{1}{Q_{ref,crit}}\frac{\partial Q_{ref,crit}}{\partial T_0} \approx -\frac{T_A}{T_0^2}. \tag{13}$$

Integration yields the change in T_0 that modifies the critical power to $Q'_{ref,crit}$

$$\Delta T_0 = -\frac{T_0}{\left(1+\frac{T_A}{T_0 \ln(Q'_{ref,crit}/Q_{ref,crit})}\right)}. \tag{14}$$

It follows that for temperatures in the range of interest the reduction in coolant temperature necessary to double the critical leakage power is given to within a few percent by $0.7 \times T_0^2/T_A$ and is typically 6.5 °C.

A study of the sensor temperature curve yields a simple geometrical relationship. From Eq. (6)

$$\left.\frac{\partial T_S}{\partial Q_{ref}}\right|_{T_S=T_0} = R_t\left(\frac{T_0}{T_{ref}}\right)^2 \exp\left(T_A\left(\frac{1}{T_{ref}} - \frac{1}{T_0}\right)\right) \tag{15}$$

and using (11) we obtain for the product $\lambda = Q_{ref,crit} \times (\partial T_S/\partial Q_{ref})|_{T_S=T_0}$

$$\lambda = T_A\left(\frac{T_0}{T_A+T_0}\right)^2 \exp\left(-\frac{1}{1+T_0/T_A}\right). \tag{16}$$

Over the range of T_0 from −30 to 10 °C, λ is 3.3 °C within ±15%. This relationship may be used to predict an approximate value for the critical power from the initial slope of the stability curve, without the need to calculate the curve completely. This can be particularly useful when optimising the geometry and material properties of a detector design.

To find the critical parameters in terms of a given leakage power we start with the coolant sink temperature to achieve a sensor temperature T_S

$$T_C = T_S - R_c Q_H - R_t Q_{ref}\left(\frac{T_S}{T_{ref}}\right)^2 \exp\left(T_A\left(\frac{1}{T_{ref}} - \frac{1}{T_S}\right)\right). \tag{17}$$

At the critical point (onset of runaway) $(\partial T_C/\partial T_S)|_{T_S=T_{S,crit}} = 0$, which yields for the critical sensor temperature

$$T_{S,crit} \approx \frac{T_{ref}}{1-\frac{T_{ref}}{T_A}\ln\left(\frac{T_{ref}^2}{R_t Q_{ref} T'_A}\right)} \tag{18}$$

where we have used $T'_A = T_A + 2T_S \approx T_A + 500\,\mathrm{K}$ (assuming that the sensor temperature T_S does not change significantly compared to T_A). This parameterization is independent of Q_H and T_C, and scales with $R_t Q_{ref}$.

Inserting this in Eq. (17) gives

$$T_{0,crit} = T_{S,crit}\left(1 - \frac{T_{S,crit}}{T'_A}\right) \tag{19}$$

which then can be used to compute the critical coolant temperature, $T_{C,crit} = T_{0,crit} - R_c Q_H$, above which runaway will occur.

The sensor-induced temperature step

$$\Delta T_{S,crit} = T_{S,crit} - T_{0,crit} = \frac{T_{S,crit}^2}{T'_A} \tag{20}$$

with a weak dependence on the thermal resistance and Q_{ref} (Fig. 7). This equation is equivalent to eq. (10). The leakage power from the sensor at the critical point is

$$Q_{crit} = \frac{\Delta T_{S,crit}}{R_t} = \frac{T_{S,crit}^2}{R_t T'_A} \tag{21}$$

with a similar weak dependence.

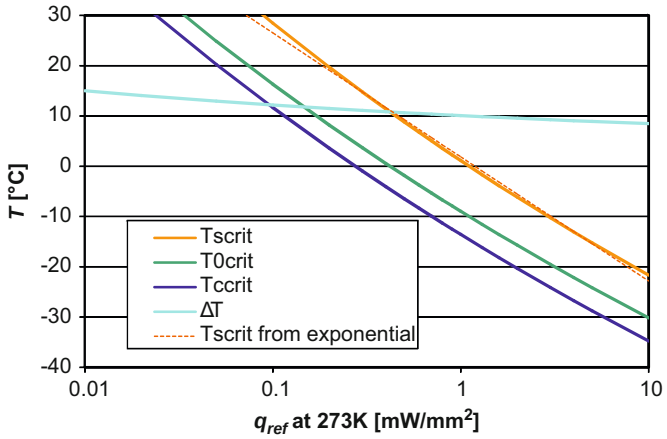

Fig. 7. Temperatures (in °C) at the critical point for the single-sided sLHC module in the minimal linear model (R_t=0.9 K/W, R_s=0, W_h=5.12 W, A_{sensor}=100 cm^2). The simple exponential leakage power dependence used to obtain the dotted line (Eqs. (22) and (23)) has been developed around a sensor temperature of 0 °C.

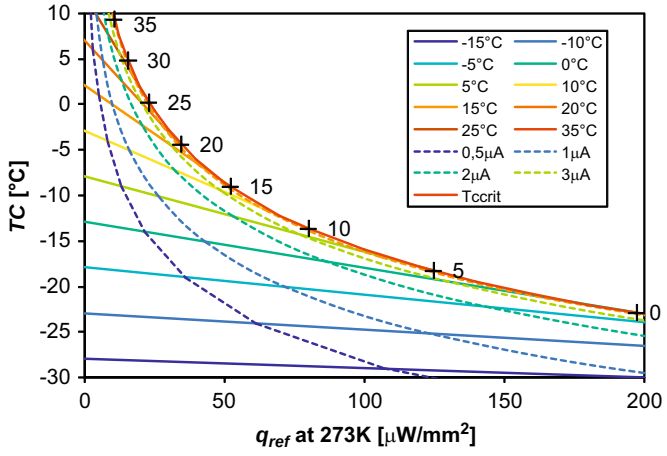

Fig. 8. Sensor isotherms (full lines) and lines of equal strip current (dashed lines) for the double-sided ATLAS barrel SCT module from the minimal model (R_s=0.945 K/W, R_c=2.164 K/W, Q_h=6 W, A_{sensor}=163 cm^2, A_{strip}=10.7 mm^2, V_{bias}=460 V). The area above the top line is excluded by thermal runaway. Crosses indicate sensor temperatures on the boundary line.

A commonly used approximation to Eq. (4) is

$$Q(T_S) = \alpha \exp((\Theta - T_S)/\beta), \quad \text{where} \tag{22}$$

$$\alpha = Q_{ref}\left(\frac{\Theta}{T_{ref}}\right)^2 \exp\left(T_A\left(\frac{1}{T_{ref}} - \frac{1}{\Theta}\right)\right), \text{ and } \beta = \frac{\Theta^2}{T_A} \tag{23}$$

where the approximation coincides with Eq. (4) at the temperature Θ. This approximation is good to $O((T_s-\Theta)/\Theta)$ close to the matching point of the two functions. However, the weak variation of ΔT_{crit} and Q_{crit} can only be found from Eq. (2). Approximating this with the simple exponential will yield constant values, β and β/R_t, respectively for Eqs. (20) and (21). This is the result quoted in Ref. [6].

Figs. 8 and 9 combine the different ways to plot thermal runaway. The boundary line to the area excluded by thermal runaway has been computed from Eqs. (18) and (19) as $T_{C,crit}(q_{ref})$. Note that the sensor temperature along the boundary line is decreasing with q_{ref} according to Eq. (18). The sensor isotherms are straight lines from Q_{ref}=0, $T_C = T_S - R_c Q_H$ to $Q_{ref,crit} = T_{ref}^2/R_t T_A' \exp(T_A/T_{ref} - T_A/T_S)$, $T_{C,crit} = T_S - R_c Q_H - T_S^2/T_A'$ on the boundary

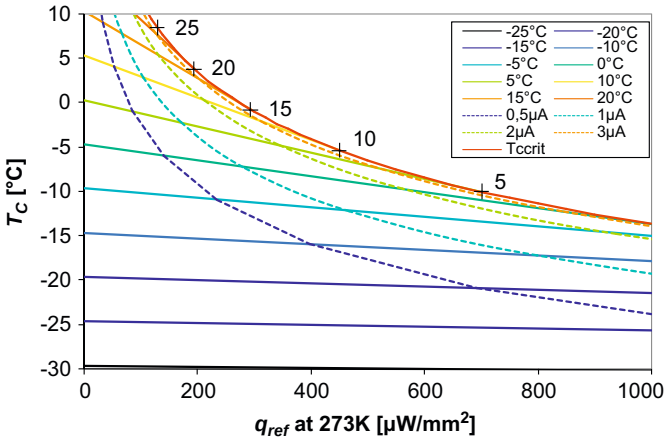

Fig. 9. Sensor isotherms (full lines) and lines of equal strip current (dashed lines) for the single-sided ATLAS sLHC short strip module from the minimal model (for this calculation we assumed R_s=0, R_c=0.9 K/W, Q_h=5.12 W, A_{sensor}=100 cm^2, A_{strip}=1.78 mm^2, V_{bias}=500 V). The area above the top line is excluded by thermal runaway. Crosses indicate sensor temperatures on the boundary line. Note the different scale for q_{ref} as compared to Fig. 8.

line. Within this range their slope is given by

$$\left(\frac{\partial T_C}{\partial Q_{ref}}\right)_{T_S} = -R_t\left(\frac{T_S}{T_{ref}}\right)^2 \exp(T_A(1/T_{ref} - 1/T_S)). \tag{24}$$

The above equations can be used to study the dependence of the critical properties on the system parameters. The critical sensor temperature varies as

$$\left(\frac{\partial T_{S,crit}}{\partial R_t}\right)_{Q_{ref}} = -\frac{T_{S,crit}^2}{R_t T_A}, \text{ and} \tag{25}$$

$$\left(\frac{\partial T_{S,crit}}{\partial Q_{ref}}\right)_{R_t} = \frac{R_t}{Q_{ref}}\left(\frac{\partial T_{S,crit}}{\partial R_t}\right)_{Q_{ref}} = -\frac{T_{S,crit}^2}{Q_{ref} T_A} \tag{26}$$

and the critical coolant temperature as

$$\left(\frac{\partial T_{C,crit}}{\partial Q_H}\right)_{Q_{ref},R_t} = -R_t \tag{27}$$

$$\left(\frac{\partial T_{C,crit}}{\partial R_t}\right)_{Q_{ref},Q_H} = -\frac{T_{S,crit}^2}{R_t T_A}\left(1 - \frac{2T_{S,crit}}{T_A'}\right) - Q_H \tag{28}$$

and

$$\left(\frac{\partial T_{C,crit}}{\partial Q_{ref}}\right)_{R_t,Q_H} = -\frac{T_{S,crit}^2}{Q_{ref} T_A}\left(1 - \frac{2T_{S,crit}}{T_A'}\right). \tag{29}$$

Integration of the latter equation allows estimating the cooling temperature change required to cope with a change in radiation damage, similarly to Eq. (14).

For comparison, far from runaway,

$$\left(\frac{\partial T_C}{\partial Q_H}\right)_{R_t,T_S} = -R_t, \left(\frac{\partial T_C}{\partial R_t}\right)_{Q_H,T_S} = -Q_H, \text{ and } \left(\frac{\partial T_C}{\partial T_S}\right)_{Q_H,R_t} = 1. \tag{30}$$

6. Estimate of temperatures and thermal stability of a thermally resistive sensor

In the minimal model we have assumed negligible temperature variations within the sensor. In reality, there are finite on- and off-sensor thermal resistances causing temperature variations in the sensor volume (see for example Fig. 1). FEA results are usually reported in terms of the temperature at the location where it is a maximum.

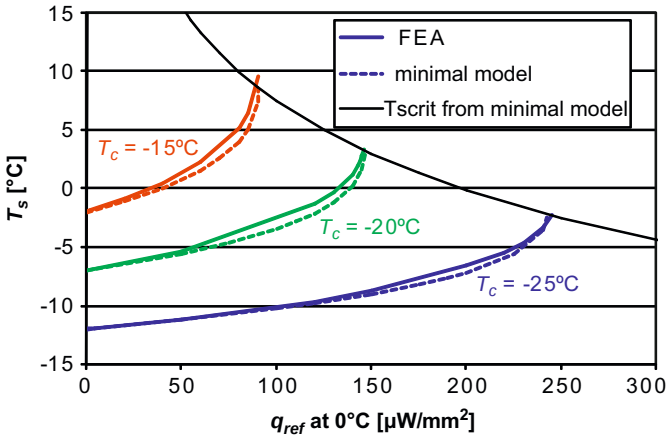

Fig. 10. Comparison of FEA for the ATLAS barrel SCT module with the critical point predictions using Eq. (10) and (12) (minimal model) for different cooling temperatures. The values for the thermal resistances used in the minimal model have been derived from the first two points of the FEA data using Eq. (31) (R_c=2.164 K/W, R_s=0.945 K/W).

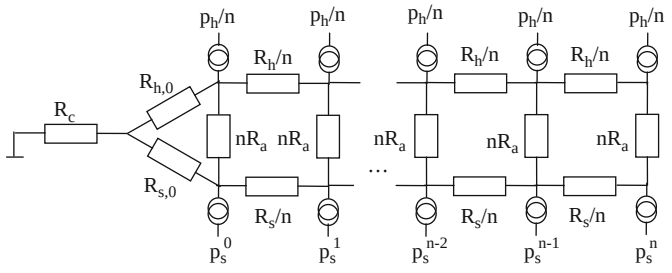

Fig. 11. Extended thermal network model.

For the minimal model the thermal resistances can be obtained from the sensor temperature curve using

$$R_C = \frac{T_0 - T_C}{Q_H} \text{ and } R_t = \frac{dT_s}{dQ_{ref}}\bigg|_{Qref\,=\,0} \times \left(\frac{T_{ref}}{T_0}\right)^2 \exp\left(T_A\left(\frac{1}{T_0} - \frac{1}{T_{ref}}\right)\right). \tag{31}$$

The same method can be used on the sensor temperature curve of a module with finite thermal sensor resistance from FEA or measurements to yield the correct value of R_c and an estimate of an average R_s with usually a reasonable agreement of the sensor temperature curve predicted by the minimal model with the data (see for example Fig. 10). Depending on the exact module geometry we find that at low leakage power the sensor temperature in the minimal model can rise faster or slower than for the thermally resistive sensor, but always rises faster close to the critical point, so that the minimum model underestimates the critical sensor temperature and often the critical leakage power.

To study the temperatures in a sensor with finite thermal resistance we have extended the thermal resistor network in our model to take into account a finite sensor resistance as well as a conductive connection over the sensor area between the readout electronics and the sensor, which in a real detector could stem from heat conduction through detector materials, wire bonds or the air gap between sensor and readout electronics, depending on the detailed detector design (Fig. 11). This models a rectangular sensor cooled all along an edge, and still is inadequate to exactly reproduce a module like the ATLAS barrel SCT module, for which the cooling contact is only over a fraction of the edge. Such truly 3-dimensional modeling we have to leave to FEA.

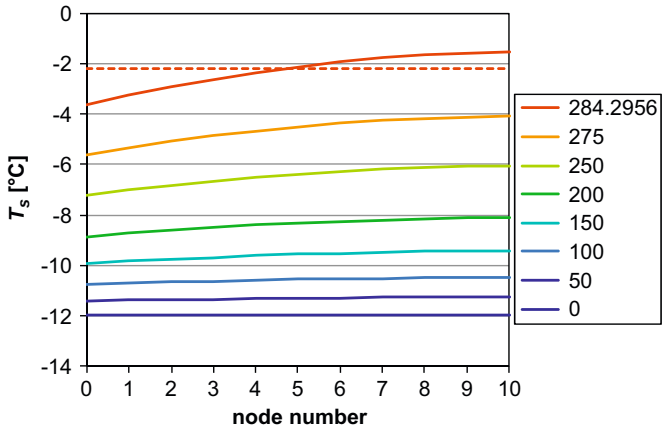

Fig. 12. Sensor temperatures in the extended network model for 11 nodes (R_c=2.17 K/W, Q_h=6 W, $R_{0,s}$=0.1 K/W, R_s=1.1 K/W, T_c=−25 °C, A_{sensor}=163 cm²) for different leakage power (in µW/mm² at 0 °C). The top most curve is the sensor temperature curve at the critical point. The dashed vertical line indicates the critical temperature from the minimal model from Eq. (10) for R_c=2.17 K/W.

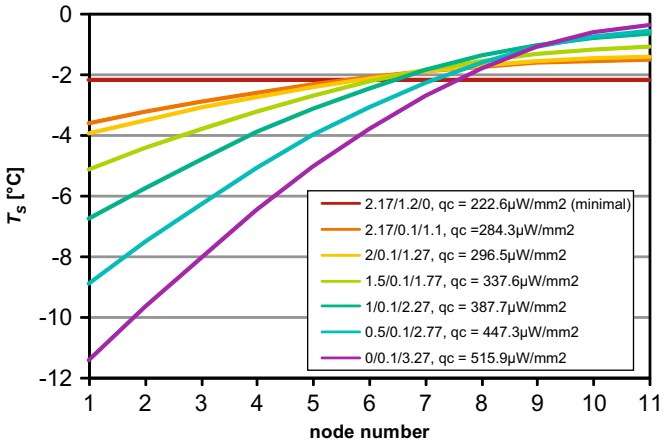

Fig. 13. Sensor temperatures at the critical point in the extended network model for 11 nodes (Q_h=6 W). The curves were computed using different thermal resistance combinations for $R_c/R_{0,s}/R_s$ (in K/W), so that the total resistance to the far sensor edge is the same. The cooling temperature was adjusted so that T_0 is identical for all curves (−11.98 °C).

There is no analytical solution for this network, but for a finite number of nodes one can set up a system of non-linear equations, for which approximate solutions can be found using a non-linear equation solver.[3]

We evaluated this set of equations for 11 nodes in the sensor for different amounts of sensor damage, first neglecting the coupling between the sensor and the readout electronics (Fig. 12). For the parameters used we find that up to the highest leakage power (at the critical point) the sensor temperature is fitted well by a parabola, the exact solution for a uniform power density,[4] although it does not satisfy the boundary condition of zero slope at the far edge of the sensor. In addition we observe that the critical sensor temperature for the minimal model as obtained in Eq. (10) is similar to the sensor temperature in the extended model at a point close to the midpoint of the sensor (Fig. 13). This model does reproduce the divergence of the minimal model from the temperature curve for finite thermal sensor resistance observed in FEA (Fig. 14).

[3] We used the findroot function in Mathematica.

[4] This dependence has been used in Ref. [3] and the validity of this assumption demonstrated in Ref. [11].

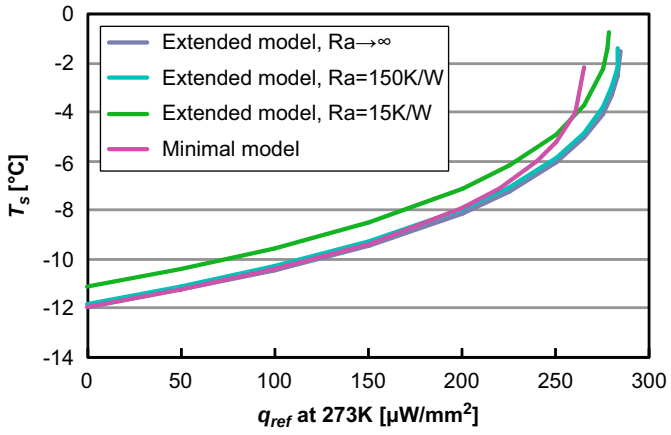

Fig. 14. Sensor temperature for the last node (maximum temperature) in the extended network (R_c=2.17 K/W, Q_h=6 W, $R_{0,s}$=0.1 K/W, R_s=1.1 K/W, $R_{0,h}$=0.1 K/W, R_h =1.1 K/W, T_c=−25 °C) and comparison to the minimal model. The parameters for the minimum model were obtained using Eq. (31) on the temperature curve for $R_a\to\infty$ (R_c=2.17 K/W, R_s=0.66 K/W).

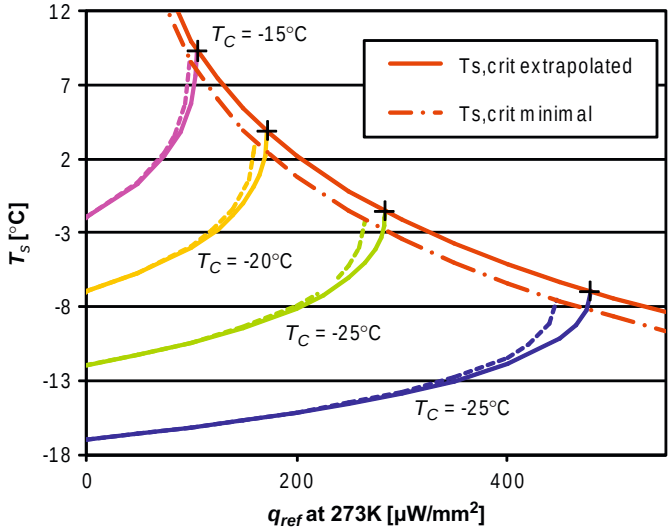

Fig. 15. Sensor temperature curves for the extended model (R_c=2.17 K/W, Q_h=6 W, $R_{0,s}$=0.1 K/W, R_s=1.1 K/W, $R_a\to\infty$) (full lines), and prediction from minimal model (R_c=2.17 K/W, R_s=0.66 K/W) for different coolant temperatures. The prediction for the thermal stability limit of the minimal model has been derived using Eq. (16), the extrapolated curve has been derived using Eq. (32) to extrapolate from the critical point for T_c=−25 °C. Crosses indicate extrapolated critical points for the different coolant temperatures.

Even though the minimal model is likely to underestimate the critical point properties the fact that it describes the temperature of some average point in the sensor makes the temperature of the hottest point on the sensor track the changes of the prediction from the minimal model. If the critical parameters for one configuration of the system are known, they can then be extrapolated with good accuracy by integrating Eqs. (25)–(29), so for example if the critical leakage power and sensor temperature are known, $Q_{ref,crit}$ and $T_{S,crit}$, then

$$T'_{S,crit} = \frac{T_{S,crit}}{1+\frac{T_{S,crit}}{T_A}\ln\frac{Q_{ref,crit}}{Q'_{ref,crit}}} \tag{32}$$

for the sensor temperatures along the thermal stability limit (Fig. 15).

7. Conclusions

For detector designs with negligible thermal resistance between different locations on the sensor we have derived a set of equations for the prediction of the onset of runaway. In particular we studied this transition depending on the (damage-dependent) sensor leakage power and the heat sink (coolant) temperature. The only other parameters required, the thermal resistances, can be derived from simple estimates of the detector geometry and material properties or, more accurately, from a limited number of FEA studies.

In particular we find that in the minimal model, for common operating parameters,

- the difference between the critical sensor temperature and T_0, the temperature of the sensor for no leakage, is about 10 °C,
- the sensor leakage power at the critical point is given approximately by 10 °C/R_t,
- the reduction in coolant temperature required to maintain thermal stability for double the leakage power is about 6.5 °C,
- the critical leakage power at the reference temperature is given by 3.3 °C divided by the slope of the sensor temperature curve at zero leakage power.

All these predictions do weakly depend on the operating parameters and apply for typical silicon detector operating conditions.

We have derived expressions which allow us to estimate the leakage power for a given set of parameters (coolant temperature and reference leakage power). This also determines the leakage current per detection element and the shot noise.

Our treatment is more general than that of Ref. [6] in that it is not restricted to temperatures close to the reference temperature Θ and is based on the physically motivated temperature dependence, rather than a local approximation. It could be equally used to derive results for the thermal performance of electronic devices at higher temperatures.

The minimal model presented in this paper underestimates the leakage power at the onset of runaway as it does not model the temperature variations across the sensor. It will therefore result in conservative predictions. Nevertheless, we have found derivatives for the critical parameters, which allow predicting the general behavior of a thermally resistive sensor with good accuracy, once the critical parameters are known for one configuration from FEA or measurements.

Acknowledgements

We would like to thank our colleagues Graham Thompson, Tony Carter, and Todd Huffman for many fruitful discussions. We gratefully acknowledge financial support from the UK Science and Technology Facilities Council.

References

[1] M. Moll, Radiation damage in silicon particle detectors, Dissertation, Hamburg, 1999, DESY THESIS-1999-040, ISSN-1435-8085.
[2] T. Kohriki, et al., IEEE Trans. Nucl. Sci. NS-43 (3) (1996) 1200.
[3] J.A. Hanlon, H.J. Ziock, Nucl. Instr. and Meth. A 370 (1996) 521, doi:10.1016/0168-9002(95)00797-0.
[4] W.O. Miller, C. Haber, A. Seiden, Thermal runaway in silicon strip detectors, ATLAS Internal Note INDET-NO-102, November 22, 1994.
[5] R. Apsimon, et al., Nucl. Instr. and Meth. A 565 (2006) 561, doi:10.1016/j.nima.2006.06.058.
[6] T. Kohriki, et al., Nucl. Instr. and Meth. A 579 (2007) 806, doi:10.1016/j.nima.2007.05.299.
[7] H. Spieler, PDG Particle Physics Booklet, July 2004, p. 267.

[8] A. Abdesselam, et al., Nucl. Instr. and Meth. A (2006).
[9] M. Cepeda, et al., Mechanical and cooling design studies for an integrated stave concept for silicon strip detectors for the super LHC, ATLAS Internal Note ATL-UPGRADE-PUB-2008-001; ATL-COM-UPGRADE-2008-001, June 10, 2008.
[10] 〈http://www.poco.com/〉.
[11] P. Ratzmann, Nucl. Instr. and Meth. A 382 (1996) 447, doi:10.1016/S0168-9002(96)00784-X.